Charge Carrier Doping As Mechanism of Self-Assembled Monolayers Functionalized Electrodes in Organic Field Effect Transistors

Article *in* Advanced Materials Interfaces · November 2021

DOI: 10.1002/admi.202101377

CITATIONS
8

READS
194

4 authors:

Kalyani Patrikar
Indian Institute of Technology Gandhinagar
6 PUBLICATIONS **18** CITATIONS
SEE PROFILE

Urvashi Bothra
University of Washington Seattle
12 PUBLICATIONS **62** CITATIONS
SEE PROFILE

V.Ramgopal Rao
Indian Institute of Technology Bombay
355 PUBLICATIONS **5,599** CITATIONS
SEE PROFILE

Dinesh Kabra
Indian Institute of Technology Bombay
145 PUBLICATIONS **4,642** CITATIONS
SEE PROFILE

ADVANCED MATERIALS INTERFACES
www.advmatinterfaces.de

Charge Carrier Doping As Mechanism of Self-Assembled Monolayers Functionalized Electrodes in Organic Field Effect Transistors

*Kalyani Patrikar, Urvashi Bothra, Valipe Ramgopal Rao, and Dinesh Kabra**

Coating electrodes with self-assembled monolayer (SAM) of polar molecules is known to reduce contact resistance (R_C) in organic field effect transistors (OFETs). It is shown that the behavior of SAM in OFETs can be explained by considering a mechanism of interfacial doping in organic semiconductor by electrodes due to charge transfer during interface formation. The enhancement is analyzed in performance of pentacene OFETs with Cu electrodes, by coating Cu with SAM of pentafluorobenzenethiol or perfluorodecanethiol. It is found that application of either SAM leads to an increase in work function of Cu surface. However, work function shift due to SAM does not correlate with trends in R_C and OFET drain current. Further, first principle calculations reveal a notable difference in delocalization of frontal orbitals with either SAM, an indicator of the difference in ease of charge transfer across interface. Based on the mechanism of interfacial doping, a semiconductor physics model is developed for estimating interface doping and injection barrier, and for predicting the consequent device characteristics. It is believed that the model and methodology developed in this study can be utilized beyond the SAM and semiconductor system used here.

1. Introduction

Organic field effect transistors (OFETs) are redefining devices and applications in domains such as sensors, RF devices, and flexible displays.[1,2] However, high operating voltages and scaling limitations are some factors preventing OFETs from realizing their commercial potential. One reason for this is the high contact resistance (R_C) encountered in OFETs at interface between source or drain electrodes and organic semiconductor (OSC) channel.[3] Mismatch in energy levels of electrode metal and OSC form an energy barrier, known as Schottky barrier, to carrier injection from source electrode to OFET channel. Schottky barrier imparts contact resistance (R_C) at interface, in series to resistance of the channel. A method to reduce R_C in OFETs is the deposition of suitable self-assembled monolayer (SAM) on contact metal surface.[4,5] SAM of polar thiolated organic molecules deposited on metal thin films have been found to shift the work function of metal surface,[6,7] and alter the energy level alignment at electrode/OSC interface.[8,9] However, the mechanism of R_C reduction by SAM is not thoroughly understood. Polar SAM has been inferred to reduce the energy barrier by imposing an opposite dipole at the interface, but it has been found that polarity of SAM does not directly relate to its effect on R_C.[10–12] SAM application is often accompanied with a positive shift in threshold voltage, reason for which is not fully clear.[13] Interfacial doping of the OSC with excess carriers by SAM functionalized electrode has been overlooked as a mechanism.[3,14] SAM treatment offers the advantage of modulating interface properties, and hence device behavior, by forming SAM of appropriate molecules. Thus, a complete understanding of mechanism can enable systematic methods to select appropriate SAM for getting required device characteristics.

Gold is most often used as electrode material in p-type OFETs as its work function ($\varphi \approx -5.1$ eV) is close to highest occupied molecular orbital (HOMO) energy level of most OSCs.[15] Metals which may be inexpensive but have a low work function, such as copper, are considered inefficient for hole injection in OFETs, as the difference in Fermi level of metal and HOMO level of OSC creates, or appends, Schottky barrier. However, significant R_C has even been reported at Au/OSC interface due to mismatch in vacuum levels across interface; in general the final energy level alignment at electrode/OSC interface cannot be predicted solely based on initial energy levels.[16,17] Pentacene, a molecular OSC, has enabled OFETs with high hole mobility.[18] SAM of PentaFluoro BenzeneThiol (PFBT) and PerFluoro DecaneThiol (PFDT) have enabled increased electrode efficiency in OFETs of solution processed OSC.[13,19–21] However, limited studies have been done to explore their effect on R_C of Cu electrodes in OFETs of evaporated molecular OSCs.

K. Patrikar, V. R. Rao
Department of Electrical Engineering
Indian Institute of Technology Bombay
Mumbai 400076, India
U. Bothra, D. Kabra
Department of Applied Physics
Indian Institute of Technology Bombay
Mumbai 400076, India
E-mail: dkabra@iitb.ac.in

The ORCID identification number(s) for the author(s) of this article can be found under https://doi.org/10.1002/admi.202101377.

DOI: 10.1002/admi.202101377

We show that the behavior of SAM in OFETs can be explained by considering interfacial doping of OSC by the functionalized electrodes during interface formation, a mechanism that is not usually associated with SAM on electrodes. We show that functionalizing Cu electrodes with SAM of PFBT or PFDT in pentacene OFETs enhances device performance. While deposition of either SAM increases the work function of Cu electrodes to a level deeper than HOMO of pentacene, OFET characteristics and R_C are significantly different for OFETs with either SAM. We find that the respective SAM molecules determine the delocalization and positions of HOMO at the interface. We show that interfacial doping correlates with these observations. Based on this mechanism, a model is developed which calculates OSC/electrode interface properties, and resulting OFET characteristics.

2. Results

2.1. Effect of SAM on Cu Surface and in OFETs

2.1.1. SAM/Cu Interface

Molecular structures of aromatic compound PFBT and alkane PFDT are shown in **Figure 1**a. Both molecules contain electronegative F, and a thiol group which forms a weak covalent bond with the Cu surface. Molecules of PFBT and PFDT are deposited in form of a SAM on Cu surface by dip coating. The formation of SAM on Cu surface, as well as absence of PFBT and PFDT on dielectric SiO_2 surface, is confirmed by X-ray photoelectron spectroscopy studies as shown in Figure S1 in the Supporting Information.

Work function (φ) of unmodified Cu as well as SAM/Cu surface, on the device stack shown in Figure 1a prior to pentacene deposition, was measured by kelvin probe microscopy (KPM). The difference between the work function of the scanning tip (φ_{tip} = −4.9 eV) and that of sample (φ_{sample}) translates to the measured contact potential difference (V_{CPD}), expressed in **Equation (1)**[23]

$$V_{CPD} = \frac{\varphi_{sample} - \varphi_{tip}}{q} \quad (1)$$

q is the electronic charge. Average V_{CPD} measured from several scans over regions of 1 μm^2 area for Cu surface is found to be 0.08 V, and hence its work function φ_{Cu} = −4.82 eV. V_{CPD} for PFBT/Cu is found to be −0.42 V, thus $\varphi_{PFBT/Cu}$ = −5.32 eV. V_{CPD} for PFDT/Cu is higher in magnitude at −0.64 V, and accordingly $\varphi_{PFDT/Cu}$ = −5.54 eV. For either SAM/Cu, the work function is higher than HOMO level of pentacene. The values of work function are summarized in **Table 1**, these match values reported previously.[24]

Table 1. Work function and OFET properties of SAM/Cu and unmodified Cu electrodes.

Electrode	φ [eV]	μ_{FET} [cm^2 V^{-1} s^{-1}]	V_T [V]
Cu	−4.82 ± 0.004	0.04 ± 0.010	−14.5 ± 1.5
PFDT/Cu	−5.54 ± 0.014	0.14 ± 0.03	0.6 ± 0.1
PFBT/Cu	−5.32 ± 0.008	0.38 ± 0.020	18.5 ± 0.4

2.1.2. OFET Characteristics

OFETs with PFBT/Cu, PFDT/Cu, or unmodified Cu electrodes were fabricated as per the schematic in Figure 1a. Transfer characteristics (I_D–V_G) for all devices is shown in Figure 1b. The

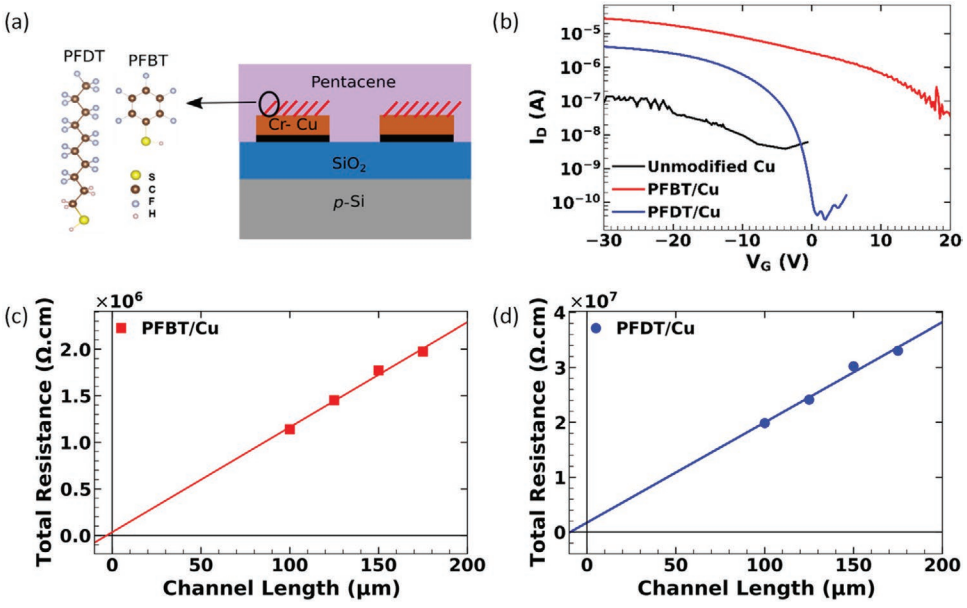

Figure 1. a) Schematic of OFET with SAM functionalized source and drain electrodes, with molecules[22] of PFBT and PFDT used for SAM. b) I_D–V_G of OFETs with electrodes as unmodified Cu, PFBT/Cu, and PFDT/Cu. Total resistance of OFETs of varying channel lengths with electrodes as c) PFBT/Cu and d) PFDT/Cu, to extract R_C from y-intercept.

values of drain current (I_D) attained by devices with PFBT/Cu or PFDT/Cu electrodes exceed I_D of devices with unmodified Cu, with I_D of devices with PFBT/Cu being higher than of OFETs with PFDT/Cu. Threshold voltage (V_T) is obtained from onset of current in I_D–V_G curves, as the value of V_G at which transistor begins to turn on. V_T of devices with PFBT/Cu (18.5 V) is significantly higher (positive) compared to PFDT/Cu (0.6 V), and with respect to OFETs with unmodified Cu. (–14.5 V). Saturation mobility (μ_{FET}) for all OFETs is extracted from linear fits of $\sqrt{I_D}$–V_G plots, based on **Equation (2)**[25]

$$\mu_{FET} = \frac{2L}{C_i W}\left(\frac{d\sqrt{I_D}}{dV_G}\right)^2 \quad (2)$$

Here W is the channel width, C_i the dielectric capacitance is 1 nF cm^{-2}. μ_{FET} for devices with PFBT/Cu (0.38 cm^2 V^{-1} s^{-1}) and that of PFDT/Cu (0.14 cm^2 V^{-1} s^{-1}), both are higher than that of OFET with unmodified Cu (0.04 cm^2 V^{-1} s^{-1}). OFET parameters are given in **Table 1**. Shift in V_T and increase in μ_{FET} are expected as per previously observed for devices with these SAM on Cu and Au electrodes.[24,26]

2.1.3. Contact Resistance

To isolate the influence of SAM functionalized electrodes on device characteristics, we obtained the contact resistance of OFETs with SAM/Cu by transfer length method (TLM).[27] The total resistance (R_{total}) of devices is obtained from I_D–V_D at low values of V_D for OFETs having different channel lengths (L). R_{total} is a sum of the channel resistance (R_{Ch}) which is a function of L, and total R_C which is independent of L, as given in Equation (3)[27]

$$R_{Total}W = R_{Ch}W + 2R_CW = \frac{L}{qn_{Ch}\mu_{FET}} + 2R_CW \quad (3)$$

Here n_{ch} the charge carrier density in channel. In the R_{total} versus L plots, the y-intercept (L = 0) represents the combined resistance at interface with source and drain. Width normalized $R_{total}W$ for OFETs with different channel lengths for V_G = –5 V, are shown in Figure 1c,d for OFETs with PFBT/Cu and PFDT/Cu. Using the linear fit of $R_{total}W$ versus L, according to Equation (3), find that value of R_CW for devices with PFBT/Cu $R_CW_{(PFBT/Cu)} = 1.7 \times 10^4$ Ω cm, while R_CW of OFETs with PFDT/Cu is higher at $R_CW_{(PFDT/Cu)} = 8.6 \times 10^5$ Ω cm. Both SAM/Cu act as Ohmic electrodes, as R_C is significantly lower than R_{Ch} for all devices. Values of R_C, found to be in the order of those previously reported for similar device configuration with Au electrodes,[26] are summarized in **Table 2**, along with R_{Ch} for OFETs with L = 100 µm.

Table 2. The calculated values of ϕ_0 and n correlate well with R_CW and $R_{Ch}W$ for L = 100 µm, in OFETs with SAM/Cu electrodes.

Electrode	R_CW [Ω cm]	$R_{Ch}W$ [Ω cm]	ϕ_0 [eV]	$n(0)$ [cm^{-3}]
PFBT/Cu	1.7×10^4	1.1×10^6	0.021	1.22×10^{21}
PFDT/Cu	8.6×10^5	1.8×10^7	0.198	1.40×10^{18}

2.2. Ab Initio Calculations on Pentacene/SAM/Cu Interface

To study the effect of PFBT and PFDT on molecular interactions at the interface, first principle calculations were performed on a section of Pentacene/SAM/Cu interface by employing Density Functional Theory (DFT). SAM/Cu surface was represented by PFBT or PFDT molecule bonded to a single layer of Cu atoms. Pentacene molecule from the first monolayer deposited on SAM/Cu surface was added to the simulated stack. The optimization of positions and orientations of components of the stack are detailed in Section S2 (Supporting Information), with the stages of calculations shown in Figures S2 and S3 in the Supporting Information.

Figure 2a shows the position of HOMO for Pentacene/PFBT/Cu system. The HOMO is highly delocalized; extending over pentacene molecule and Cu atoms of thin film, along with C atoms of PFBT molecule. The delocalization of HOMO facilitates hole transfer across the interface. Figure 2b shows the location of HOMO for Pentacene/PFDT/Cu system, with HOMO localized specifically over pentacene molecule. Unlike PFBT molecule, mediation by PFDT molecule does not lead to delocalization of HOMO throughout the interface, and does not favor hole transfer to as great an extent.

3. Discussion

Values of I_D for OFETs with PFBT/Cu is higher than for OFETs with PFDT/Cu, in spite of values of μ_{FET} being close. Also, value of R_C is lower for OEFTs with PFBT/Cu than for OFETs with PFDT/Cu. This is contradictory to the trends in φ, where PFDT/Cu attain higher values than PFBT/Cu. This indicates that the work function tuning of copper surface does not explain completely the mechanism of electrode functionalization by a polar SAM. SAM is known to have an effect on the morphology of OSC deposited on it.[28] However, as explained in Section S3 in the Supporting Information, we observe no significant difference in long range ordering of pentacene in devices with either SAM as per the X-ray diffraction spectra shown in Figure S4 (Supporting Information) and atomic force microscope (AFM) analysis in Figure S5 in the Supporting Information. The positions of frontal molecular orbitals at interface, as obtained from first principle calculations, reveal the ease of acquisition of excess holes by pentacene at Pentacene/PFBT/Cu interface, as compared to Pentacene/PFDT/Cu, correlating with observed I_D and R_C. We proceed to analyze the mechanism of SAM functionalized electrodes and their influence on device behavior.

3.1. Mechanism of SAM Functionalized Electrodes in OFETs

A lower V_T and higher R_C of OFETs with PFDT/Cu electrodes indicates a high Schottky barrier at Pentacene/PFDT/Cu interface,[29] while a lower R_{Ch} in OFETs with PFBT/Cu electrodes and higher I_D at V_G = 0 V suggests a low Schottky barrier at Pentacene/PFBT/Cu interface.[29] OFETs with either SAM have a positive V_T, which we consider to indicate presence of excess holes in pentacene at equilibrium.[30] As the channel and dielectric are identical for devices with either SAM, we surmise that the excess hole density is due to SAM at the interface. These excess

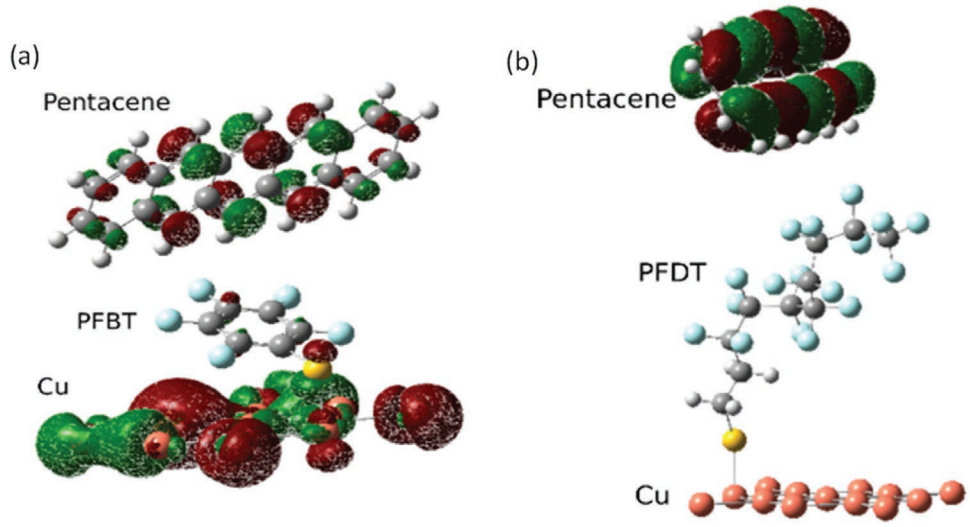

Figure 2. Locations of HOMO of a) Pentacene/PFBT/Cu system and b) Pentacene/PFDT/Cu system exhibiting the difference in orbital delocalization at interface.

accumulated holes get depleted upon applying Gate voltage $V_G = V_T$. Depletion results from an equal and opposite charge imposed on the dielectric surface by V_T, magnitude of which is $C_i V_T$ cm^{-2}.[31,32] Considering the hole density in pentacene at equilibrium to be n at distance x from the interface, its magnitude can be obtained based on value of V_T as given by **Equation (4)**

$$2qt\int_0^{L/2} n(x)\,dx = C_i V_T L \tag{4}$$

Here t is the thickness of the pentacene film.

Excess holes in OSC is a consequence of the phenomenon related to energy level alignment of SAM/Cu and pentacene during interface formation.[3,15] Fermi level of SAM/Cu is higher (negative) than that of pentacene. Thus, at the onset of interface formation there is a transfer of electrons from OSC to electrode, as illustrated in **Figure 3**a, leaving behind hole carrying pentacene cations with density n, decreasing with x. n is accompanied by development of a built in potential ($\phi(x)$) in pentacene, which causes bending of HOMO levels. The charge transfer is expected to stop when fermi levels of both materials align, presumably at midgap of pentacene. However, due

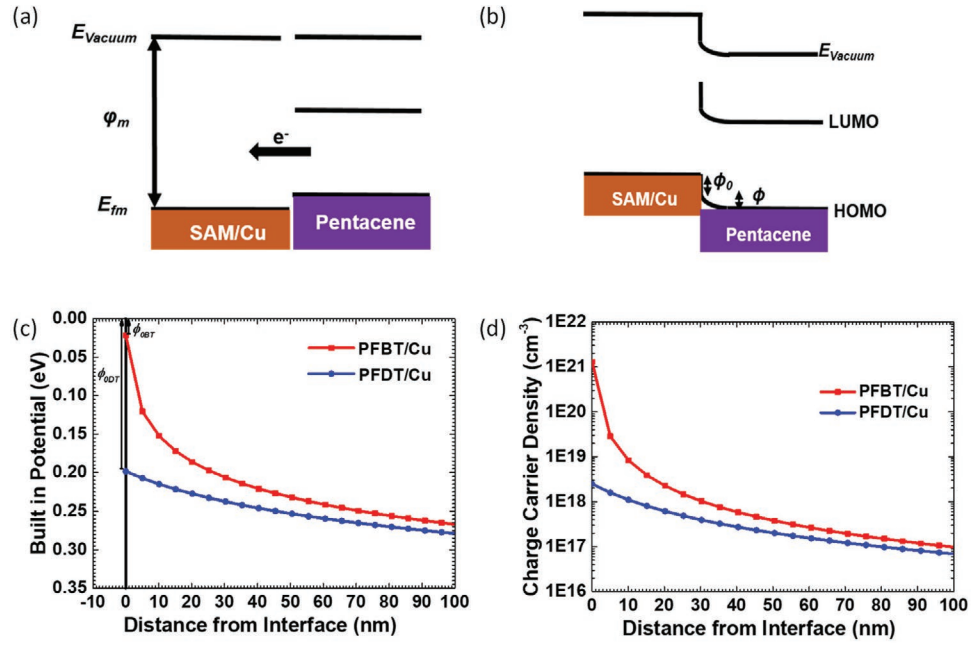

Figure 3. Schematic of a) charge transfer during interface formation and b) equilibrium energy level alignment. c) Built in potential (ϕ) profile in pentacene at equilibrium up to $x = 100$ nm from electrode interface, along with Schottky barrier ϕ_0 (ϕ at $x = 0$) marked d) the corresponding excess charge carrier density (n) profile in pentacene, for OFETs with either SAM/Cu.

to various phenomenon involved with interaction of electrode and OSC, equilibrium is established with pinning of electrode Fermi level deeper than the midgap of Pentacene.[3,15] Further, a mismatch of respective vacuum levels occurs at interface, causing the formation of an interfacial dipole, which constitutes Schottky barrier (ϕ_0). The equilibrium energy levels are as shown in Figure 3b, with an energy barrier of height ϕ_0 at Pentacene/SAM/Cu interface, and pentacene carrying a built-in potential ($\phi(x)$) and an excess accumulated hole density ($n(x)$).

Combining Poisson's equation, with boundary conditions at the interface, gives the relation between $n(x)$ and $\phi(x)$ within pentacene at equilibrium, given by **Equation (5)**[31]

$$\frac{\partial^2\phi(x)}{\partial x^2} = \frac{q}{\varepsilon\varepsilon_0} n(x); \quad n(0) = N e^{-\frac{q\phi_0}{kT}}, \ \lim_{x\to\infty}\left(\frac{\mathrm{d}\phi}{\mathrm{d}x}\right) = 0 \tag{5}$$

Here N the pentacene site density is 3×10^{21} cm^{-3},[33] k is the Boltzmann constant, T is the temperature, ε_0 is the permittivity of vacuum, and ε_s the dielectric constant of pentacene is 3.6.[34] With given conditions at interface of pentacene and SAM/Cu, solution for Equation (5) takes the form given in **Equation (6)**[31]

$$n(x) = N\left[e^{\frac{-\phi_0 q}{2kT}} + xq\sqrt{\frac{N}{2kT\varepsilon_0\varepsilon_s}}\right]^{-2} \tag{6a}$$

$$\phi(x) = \frac{2kT}{q}\ln\left[e^{\frac{-\phi_0 q}{2kT}} + xq\sqrt{\frac{N}{2kT\varepsilon_0\varepsilon_s}}\right] \tag{6b}$$

Solving Equations (4) and (6) simultaneously for $L = 100$ µm gives the equilibrium profiles of ϕ and n in pentacene for OFETs with PFBT/Cu and PFDT/Cu, as shown in Figure 3c,d for $x = 0$ to $x = 100$ nm. ϕ_0 calculated for Pentacene/PFBT/Cu $\phi_{0(\mathrm{PFBT/Cu})} = 0.021$ eV is significantly lower than for Pentacene/PFDT/Cu $\phi_{0(\mathrm{PFDT/Cu})} = 0.198$ eV. PFDT functionalized electrodes forms an interface with a larger value of ϕ_0, as has been previously observed with PFDT/Au.[35] In case of either SAM, ϕ_0 is lower than that reported for unmodified Cu electrodes.[17] Values of charge carrier density in pentacene at interface for PFBT/Cu $n_{\mathrm{PFBT/Cu}}(0) = 1.22 \times 10^{21}$ cm^{-3}, is markedly higher than for PFDT/Cu $n_{\mathrm{PFDT/Cu}}(0) = 1.40 \times 10^{18}$ cm^{-3}. Charge carrier density averaged over L for PFBT/Cu OFETs is $\tilde{n}_{\mathrm{PFBT/Cu}} = 2.27 \times 10^{16}$ cm^{-3} and for PFDT/Cu OFETs is $\tilde{n}_{\mathrm{PFDT/Cu}} = 7.48 \times 10^{14}$ cm^{-3}. Interface properties are summarized in Table 2, values of $\tilde{n}$ for OFETs for varied L are given in Table S1 in the Supporting Information. The calculated values of n of respective SAM/Cu correlate well with trends observed in I_D, R_{Ch}, and R_C. Values of $\tilde{n}$ are also consistent with the observed values of μ_{FET}.[36] Larger orbital delocalization at Pentacene/PFBT/Cu interface as compared to Pentacene/PFDT/Cu interface (Section 2.2.) explains the difference in ϕ_0 and n for devices with either SAM.

3.2. Device Characteristics of SAM Functionalized Electrodes

Based on the values of n obtained from above analysis, linear regime of output characteristics are derived by applying the gradual channel approximation,[37] and including the excess carriers due to interfacial doping, as given in Equation (7)

$$I_D = q\tilde{n}t\frac{\mu W}{L}V_D + C_i\left(V_G - \frac{V_D}{2}\right)\frac{\mu W}{L}V_D \tag{7}$$

In case of PFBT/Cu devices, the high density of excess carriers causes the voltage drop across channel to change in proportion to the charges depleted by the effect of V_D. Rather than transition to an abrupt pinch-off, the charge carrier density and effective drain voltage decrease gradually until saturation is attained. This effective V_D acting across the channel is represented as the parameter channel voltage (V_{Ch}), given by

$$V_{Ch} = \frac{q\tilde{n}t - C_i V_D/2}{q\tilde{n}t}V_D \tag{8}$$

I_D here is expressed in Equation (9).

$$I_D = q\tilde{n}t\frac{\mu W}{L}V_{Ch} + \frac{\mu W}{L}C_i(V_G - V_{Ch})V_{Ch} \tag{9}$$

When the value of V_D achieves complete depletion of carriers at drain, the OFET achieves condition of saturation, beyond which I_D is nearly independent of V_D, as per Equation (10).

$$I_D = \frac{\mu W}{2L}C_i\left(V_G + q\tilde{n}t/C_i\right)^2(1 + \lambda V_D) \tag{10}$$

Where λ is an empirical parameter.[38] For V_G varying from 0 to −10 V, the I_D–V_D are estimated by Equations (7) and (9) or (10) depending on the regime of operation and values of $\tilde{n}$. As shown in **Figure 4**a,b, these estimated I_D–V_D for PFBT/Cu and PFDT/Cu match experimental values well. Fits for devices with varied L are shown in Figure S6 in the Supporting Information. As the estimated I_D–V_D depend on values of $\tilde{n}$ obtained as per model discussed in Section 3.1., the close match between estimated and experimental values asserts the importance of interfacial doping in influencing device behavior for OFETs with SAM functionalized electrodes.

4. Conclusion

Functionalization of Cu electrodes with SAM of PFBT or PFDT enhances performance of pentacene OFETs. Work function of Cu surface was found to increase from −4.82 eV, to higher values with $\varphi_{\mathrm{PFDT/Cu}} = -5.54$ eV and $\varphi_{\mathrm{PFBT/Cu}} = -5.32$ eV. In contrast to these trends, contact resistance of OFETs at $V_G = -5$ V with PFBT/Cu $R_C W_{(\mathrm{PFBT/Cu})} = 1.71 \times 10^4$ Ω cm is lower than with PFDT/Cu $R_C W_{(\mathrm{PFDT/Cu})} = 8.56 \times 10^5$ Ω cm. We show that characteristics of OFETs can be explained considering the interface doping by SAM/Cu due to charge transfer during interface formation. Magnitude of charge transfer is calculated based on V_T, and according to solution of Poisson's equation for Pentacene/SAM/Cu interface. Interface hole density at equilibrium in OFETs with PFBT/Cu $n(0)_{\mathrm{PFBT/Cu}} = 1.22 \times 10^{21}$ cm^{-3} is higher than with PFDT/Cu $n(0)_{\mathrm{PFDT/Cu}} = 2.49 \times 10^{18}$ cm^{-3}. The Schottky barrier in OFETs with PFBT/Cu $\phi_{0(\mathrm{PFBT/Cu})} = 0.021$ eV

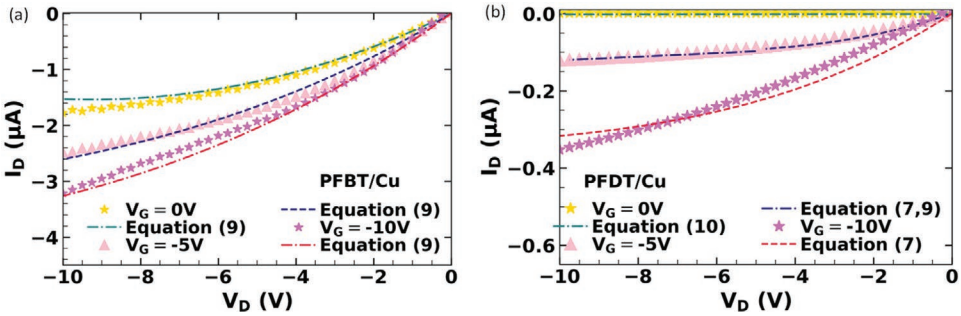

Figure 4. Experimental I_D–V_D along with calculated I_D–V_D as per respective values of V_G, for OFETs with a) PFBT/Cu and b) PFDT/Cu electrodes.

is lower than with PFDT/Cu $\phi_{0(PFDT/Cu)}$ = 0.198 eV. Applying DFT based calculations, we find that the HOMO orbitals of the Pentacene/PFBT/Cu system is highly delocalized as compared to HOMO of Pentacene/PFDT/Cu system, which facilitates a larger hole transfer to pentacene from electrodes with PFBT/Cu, found to be consistent with our calculations. Further, we find I_D–V_D estimated using the values of n obtained to correlate well with the experimental device characteristics. Thus, we establish a method to predict the interface properties of SAM functionalized electrodes, along with interface doping, based on OFET transfer characteristics. We show that the effect of SAM on orbital position at interface has a significant influence on resulting device characteristics. Our results and analysis shift the usual paradigm on mechanism of SAM functionalized in OFETs, stressing on the contribution of equilibrium charge transfer rather than work function tuning, or solely energy level alignment, in enhancing device performance. This will enable better design and selection of SAM molecules for electrode interlayers.

5. Experimental Section

Device Fabrication: OFETs were prepared on (100) p-type low resistivity Si substrates which acted as Gate. A 200 nm oxide dielectric layer was grown on Si by thermal oxidation. 3nm Cr as adhesion layer, followed by 40nm Cu films, were deposited by thermal evaporation in an MBraun nitrogen glove box using Cr powder and Cu shavings respectively, through stencils having patterns of channel width 5mm and varied channel lengths. Compounds 2,3,4,5,6-Pentafluorothiophenol (C_6F_5SH) for PFBT SAM and 3,3,4,4,5,5,6,6,7,7,8,8,9,9,10,10,10-Heptadecafluoro-1-decanethiol ($C_{10}F_{17}H_5S$) for PFDT SAM, were obtained from Sigma Aldrich. Samples were immediately transferred from Glove Box after thermal evaporation of metals, and immersed in 0.5×10^{-3} M solutions of PFBT or PFDT in ethanol for 90 min, followed by ultrasonication rinsing in ethanol and then isopropyl alcohol. 50nm pentacene was deposited by thermal evaporation at a vacuum of 3×10^{-6} mbar, using Pentacene ($C_{22}H_{14}$) powder obtained from Sigma Aldrich.

Material and Electrical Characterization: X-ray photoelectron spectroscopy was carried out on Axis Supra surface analytical facility, with a 1486.6 eV monochromatic X-ray source. Kelvin Probe Microscopy was carried out on MFP3D Origin AFM, with Ti–Ir coated tip. Electrical measurements on OFETs were performed using Keithley 4200 SCS system with Semi-probe station inside nitrogen glovebox. X-ray Diffraction was carried out on a Rigaku High Resolution X Ray Diffractometer with Cu $K\alpha 1$ optics.

Computation Methods: Initial optimization was done using Quantum Espresso,[39,40] with plane wave basis set and PAW–PBE exchange–correlation functional.[41–43] Convergence was set to 10^{-8} eV. All the calculations were performed using a single k-point in Brillouin zone (BZ), at the Γ-point. DFT based calculations for optimization of position of pentacene and calculation of molecular orbitals, were carried out using Gaussian09 with B3LYP level of theory, using 6–31G basis set.[44–47] Convergence was set to 10^{-8} eV.

Supporting Information

Supporting Information is available from the Wiley Online Library or from the author.

Acknowledgements

The authors acknowledge Center for Excellence in Nanoelectronics, Indian Institute of Technology Bombay, for providing experimental facilities and funding. The authors acknowledge c-AFM, Indian Institute of Technology Bombay. The authors also acknowledge DST/INT/SWD/VRP-20/2019 Science and Engineering Research Board, Government of India.

Conflict of Interest

The authors declare no conflict of interest.

Data Availability Statement

The data that support the findings of this study are available from the corresponding author upon reasonable request.

Keywords

contact resistance, interfacial doping, self-assembled monolayers, work function

Received: July 30, 2021
Revised: September 28, 2021
Published online:

[1] M. C. Gwinner, D. Kabra, M. Roberts, T. J. K. Brenner, B. H. Wallikewitz, C. R. Mcneill, R. H. Friend, *Adv. Mater.* **2012**, *24*, 2728.
[2] J. Krumm, *(Proceedings of) 4th European Workshop on RFID Systems and Technologies* **2008**, p. 1.
[3] D. Natali, M. Caironi, *Adv. Mater.* **2012**, *24*, 1357.

[4] I. H. Campbell, S. Rubin, T. A. Zawodzinski, J. D. Kress, R. L. Martin, D. L. Smith, N. N. Barashkov, J. P. Ferraris, *Phys. Rev. B* **1996**, *54*, R14321.
[5] S. Satti, T. Naik, V. Lakshmi, M. Ravikanth, V. R. Rao, *IEEE 15th International Conference on Nanotechnology (Proceedings of IEEE Nano)* **2015**, p. 537.
[6] K. Wu, S. Yu, Y. Tao, *Langmuir* **2009**, *25*, 6232.
[7] D. Boudinet, M. Benwadih, Y. Qi, S. Altazin, J. Verilhac, M. Kroger, C. Serbutoviez, R. Gwoziecki, R. Coppard, G. Le, A. Kahn, *Org. Electron.* **2010**, *11*, 227.
[8] K. Hong, J. W. Lee, S. Y. Yang, K. Shin, H. Jeon, S. H. Kim, C. Yang, C. E. Park, *Org. Electron.* **2008**, *9*, 21.
[9] H. Vazquez, F. Flores, A. Kahn, *Proc. Int. Symp. Super-Funct. Org. Devices* **2005**, 1.
[10] P. Marmont, N. Battaglini, P. Lang, G. Horowitz, J. Hwang, A. Kahn, C. Amato, P. Calas, *Org. Electron.* **2008**, *9*, 419.
[11] A. Risteska, S. Steudel, M. Nakamura, D. Knipp, *Org. Electron.* **2014**, *15*, 3723.
[12] K. Asadi, F. Gholamrezaie, E. C. P. Smits, P. W. M. Blom, B. De Boer, *J. Mater. Chem.* **2007**, *17*, 1947.
[13] C. H. Kim, H. Hlaing, F. Carta, Y. Bonnassieux, G. Horowitz, I. Kymissis, *ACS Appl. Mater. Interfaces* **2013**, *5*, 3716.
[14] M. Waldrip, O. D. Jurchescu, D. J. Gundlach, E. G. Bittle, *Adv. Funct. Mater.* **2019**, *30*, 1904576.
[15] J. Hwang, A. Wan, A. Kahn, *Mater. Sci. Eng.* **2009**, *64*, 1.
[16] F. Amy, C. Chan, A. Kahn, *Org. Electron.* **2005**, *6*, 85.
[17] B. Jaeckel, J. B. Sambur, B. A. Parkinson, *J. Appl. Phys.* **2008**, *103*, 603719.
[18] C. Y. Han, W. M. Tang, P. T. Lai, *IEEE Trans. Electron Devices* **2017**, *64*, 1716.
[19] F. Gholamrezaie, K. Asadi, R. A. Kicken, B. M. Langeveld–voss, D. M. De Leeuw, P. W. Blom, *Synth. Met.* **2011**, *161*, 2226.
[20] C.-H. Kim, H. Hlaing, J.-A.m Hong, J.i-H. Kim, Y. Park, M. M. Payne, J. E. Anthony, *Adv. Mater. Interfaces* **2015**, *2*, 1400384.
[21] Y. Y. Noh, X. Cheng, M. Tello, M. J. Lee, H. Sirringhaus, *Semicond. Sci. Technol.* **2011**, *26*, 034003.
[22] K. Momma, F. Izumi, *J. Appl. Crystallogr.* **2011**, *44*, 1272.
[23] W. Melitz, J. Shen, A. C. Kummel, S. Lee, *Surf. Sci. Rep.* **2011**, *66*, 1.
[24] A. V. Masurkar, *Charge Injection and Transport in Pentacene Field -Effect Transistors*, Columbia University (Thesis) **2017**.
[25] G. Horowitz, *Adv. Mater.* **1998**, *10*, 365.
[26] P. Tardy, G. Wantz, Y. Nicolas, L. Vellutini, *Appl. Phys. Lett.* **2012**, *100*, 33.
[27] H. Klauk, G. Schmid, W. Radlik, W. Weber, L. Zhou, C. D. Sheraw, J. A. Nichols, T. N. Jackson, *Solid-State Electron.* **2003**, *47*, 297.
[28] B. K. Asadi, Y. Wu, F. Gholamrezaie, P. Rudolf, P. W. M. Blom, *Adv. Mater.* **2009**, *21*, 4109.
[29] Y. Xu, H. Sun, Y. Noh, *IEEE Trans. Electron Devices* **2017**, *64*, 1932.
[30] S. D. Wang, T. Miyadera, T. Minari, Y. Aoyagi, K. Tsukagoshi, *Appl. Phys. Lett.* **2008**, *93*, 2008.
[31] I. G. Lezama, A. F. Morpurgo, *Phys. Rev. Lett.* **2009**, 103, 066803.
[32] R. Schroeder, L. A. Majewski, M. Grell, *Appl. Phys. Lett.* **2003**, *83*, 3201.
[33] D. V. Lang, X. Chi, T. Siegrist, A. M. Sergent, A. P. Ramirez, *Phys. Rev. Lett.* **2004**, *93*, 8.
[34] C. H. Kim, O. Yaghmazadeh, D. Tondelier, Y. B. Jeong, Y. Bonnassieux, G. Horowitz, *J. Appl. Phys.* **2011**, *109*, 083710.
[35] X. Cheng, Y. Y. Noh, J. Wang, M. Tello, J. Frisch, R. P. Blum, A. Vollmer, J. P. Rabe, N. Koch, H. Sirringhaus, *Adv. Funct. Mater.* **2009**, *19*, 2407.
[36] J. Zhou, Y. C. Zhou, J. M. Zhao, C. Q. Wu, X. M. Ding, X. Y. Hou, *Phys. Rev. B* **2007**, *75*, 153201.
[37] M. Weis, *J. Appl. Phys.* **2012**, *111*, 054506.
[38] J. N. Haddock, X. Zhang, S. Zheng, Q. Zhang, S. R. Marder, B. Kippelen, *Org. Electron.* **2006**, *7*, 45.
[39] P. Giannozzi, S. Baroni, N. Bonini, M. Calandra, R. Car, C. Cavazzoni, D. Ceresoli, G. L. Chiarotti, M. Cococcioni, I. Dabo, A. Dal Corso, S. de Gironcoli, S. Fabris, G. Fratesi, R. Gebauer, U. Gerstmann, C. Gougoussis, A. Kokalj, M. Lazzeri, L. Martin–Samos, N. Marzari, F. Mauri, R. Mazzarello, S. Paolini, A. Pasquarello, L. Paulatto, C. Sbraccia, S. Scandolo, G. Sclauzero, A. P. Seitsonen, A. Smogunov, P. Umari, R. M. Wentzcovitch, *J. Phys.: Condens. Matter* **2009**, *21*, 395502.
[40] P. Giannozzi, O. Andreussi, T. Brumme, O. Bunau, M. B. Nardelli, M. Calandra, R. Car, C. Cavazzoni, D. Ceresoli, M. Cococcioni, N. Colonna, I. Carnimeo, A. D. Corso, S. de Gironcoli, P. Delugas, R. A. D. Jr., A. Ferretti, A. Floris, G. Fratesi, G. Fugallo, R. Gebauer, U. Gerstmann, F. Giustino, T. Gorni, J. Jia, M. Kawamura, H.–Y. Ko, A. Kokalj, E. Küçükbenli, M. Lazzeri, M. Marsili, N. Marzari, F. Mauri, N. L. Nguyen, H.–V. Nguyen, A. Otero–de–la–Roza, L. Paulatto, S. Poncé, D. Rocca, R. Sabatini, B. Santra, M. Schlipf, A. P. Seitsonen, A. Smogunov, I. Timrov, T. Thonhauser, P. Umari, N. Vast, X. Wu, S. Baroni, *J. Phys.: Condens. Matter* **2017**, *29*, 465901.
[41] G. Kresse, D. Joubert, *Phys. Rev. B* **1999**, *59*, 1758.
[42] P. E. Blöchl, *Phys. Rev. B* **1994**, *50*, 17953.
[43] J. P. Perdew, K. Burke, M. Ernzerhof, *Phys. Rev. Lett.* **1996**, *77*, 3865.
[44] M. J. Frisch, G. W. Trucks, H. B. Schlegel, G. E. Scuseria, M. A. Robb, J. R. Cheeseman, G. Scalmani, V. Barone, G. A. Petersson, H. Nakatsuji, X. Li, M. Caricato, A. V. Marenich, J. Bloino, B. G. Janesko, R. Gomperts, B. Mennucci, H. P. Hratchian, J. V. Ortiz, A. F. Izmaylov, J. L. Sonnenberg, D. Williams–Young, F. Ding, F. Lipparini, F. Egidi, J. Goings, B. Peng, A. Petrone, T. Henderson, D. Ranasinghe, V. G. Zakrzewski, J. Gao, N. Rega, G. Zheng, W. Liang, M. Hada, M. Ehara, K. Toyota, R. Fukuda, J. Hasegawa, M. Ishida, T. Nakajima, Y. Honda, O. Kitao, H. Nakai, T. Vreven, K. Throssell, J. A. Montgomery Jr., J. E. Peralta, F. Ogliaro, M. J. Bearpark, J. J. Heyd, E. N. Brothers, K. N. Kudin, V. N. Staroverov, T. A. Keith, R. Kobayashi, J. Normand, K. Raghavachari, A. P. Rendell, J. C. Burant, S. S. Iyengar, J. Tomasi, M. Cossi, J. M. Millam, M. Klene, C. Adamo, R. Cammi, J. W. Ochterski, R. L. Martin, K. Morokuma, O. Farkas, J. B. Foresman, D. J. Fox, *Gaussian, Inc.*, Wallingford CT **2016**.
[45] A. D. Beck, *Phys. Rev. A.* **1988**, *38*, 3098.
[46] C. Lee, W. Yang, R. G. Parr, *Phys. Rev. B* **1988**, *37*, 785.
[47] R. Ditchfield, W. J. Hehre, J. A. Pople, *J. Chem. Phys.* **1971**, *54*, 724.